

# A FRACTURE MECHANICS ANALYSIS OF MULTIPLE CRACKING IN COATINGS<sup>†</sup>

JOHN A. NAIRN and SUNG-RYONG KIM

*Department of Materials Science & Engineering, University of Utah,  
Salt Lake City, Utah 84112*

**Abstract**—Recent variational mechanics analysis of composite microcracking (J. A. Nairn, *J. Comp. Mat.*, **23**, 1106 (1989)) has been modified to predict the onset and propagation of multiple cracking in brittle coatings. In the modified analysis, we derived an expression for the total energy released due to the formation of a new crack across the entire cross section of the coating. Under the assumption that the next coating crack will occur when the energy released on forming that crack reaches the critical energy release rate of the coating (the coating fracture toughness), the new analysis can be used to predict the strain required to form the first coating crack and to predict the coating crack density as a function of increasing applied strain. The predictions were compared to literature results on brittle stress analysis coatings and to experimental results on poly(methyl methacrylate) coatings applied to General Electric Lexan<sup>®</sup> polycarbonate substrates. The agreement between theory and experiment was good.

## INTRODUCTION

Paints and other types of coatings are often used to decorate, to protect, or to otherwise alter the surface properties of materials. A common characteristic of many coatings is that they are more brittle than the substrate to which they are applied. For example, many paints derive their color by using an added pigment; the added pigment often embrittles the paint's binder polymer. When a substrate coated with a relatively more brittle coating is stressed, the first form of failure will be a crack in the coating. This crack will typically initiate and rapidly propagate through the entire thickness of coating. When the crack reaches the coating/substrate interface, it has several alternative failure modes:

*Surface Embrittlement:* The coating crack can continue into the substrate and cause complete structural failure. This crack path has been observed in coated polymers. Otherwise ductile polymers can be rendered brittle by the application of relatively thin coatings of brittle polymers [1-3].

*Coating Delamination:* The coating crack can change direction and propagate along the interface between the substrate and the coating. This path would be expected for coatings that are poorly adhered to the substrate.

*Multiple Cracking:* The coating crack can become arrested. Further loading of the sample will cause additional cracks in the coating. If the coating cracks continue to be arrested, the result will be multiple cracks in the coating. Multiple cracking is a common mode of failure for paints and results in a degradation in the appearance.

---

<sup>†</sup> This author-prepared reprint corrects a factor of 2 error for  $Y(D)$  in Eq. (37) that appears in the printed version. The factor of 2 correction is also made to all other equations involving  $Y(D)$  and to coating toughness values determined by fits that relied on  $Y(D)$ . The conclusions of the paper are not affected.

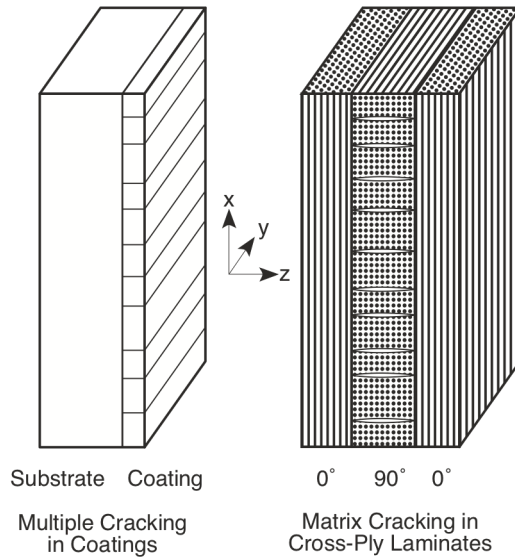


Fig. 1: There is a close analogy between multiple cracking in coatings applied to substrates and matrix microcracking in the  $90^\circ$  plies in cross ply laminates ( $[0_n/90_m]_s$ ). The left side shows cracks in a brittle coating and the right side shows cracks in  $90^\circ$  plies.

To fully understand the failure of coatings, we must analyze each of these possible failure modes. In this paper, we consider only multiple cracking failures.

The phenomenon of multiple cracking of coatings has a close analogy in the phenomenon of matrix microcracking in composite materials. As illustrated in Fig. 1, as cross-ply laminates are loaded in tension ( $[0_n/90_m]_s$  laminates), the first form of failure is transverse cracking across the cross-section of the  $90^\circ$  plies. These transverse or matrix microcracks are usually arrested at the interface between the  $0^\circ$  and the  $90^\circ$  plies. Further loading causes multiple microcracking until eventually other damage mechanisms such as delamination and fiber fracture occur resulting in complete laminate failure [4-11].

The analogy between matrix microcracking in composites and multiple cracking in coatings suggests adopting techniques used in analyzing matrix microcracking to the analysis of coating failures. Several analytical models have been proposed for matrix microcracking. Some of these models have been based a lamina strength [5,9,12,13] and postulate that the  $90^\circ$  plies (the brittle layer) fail when the strain in those plies reaches some critical value. Experimental results, however, show that the strain in the  $90^\circ$  plies at time of failure is not a material constant but rather depends on such variables as the thickness of the  $90^\circ$  plies [14]. Similar empirical approaches have been used to predict failure of brittle coatings that are used for stress analysis of structures [15]. Following a calibration experiments, the brittle coatings are postulated to fail when the strain in the coating reaches some critical value. Again, this critical value is known to depend on non-material variables such as coating thickness, substrate thickness, and technique of application [15]. In brief, the strength based models of matrix microcracking or brittle coating failures are not appropriate and can not predict failure in structures of arbitrary construction.

Better results on predicting matrix microcracking have been obtained by using fracture mechanics or strain energy release rate based models [8,10,11,16-19]. In brief, these models

postulate the the crack in the 90° plies forms when the energy release associated with the formation of that crack reaches some critical value - the *in situ* fracture toughness of the 90° plies. Early energy release rate analyses [8,10,11,16,17] were too qualitative to be useful. These analyses used inappropriate shear-lag approximations and did a poor job of incorporating residual thermal stresses [18]. We have recently derived an improved fracture mechanics analysis [18,19] that is based on more accurate, albeit still approximate, variational mechanics solution of the stresses in multilayered structures [20,21]. In this paper we describe an adaptation of the previous composite matrix microcracking analysis in ref. [18] to analyze the phenomenon of multiple cracking in paints or coatings applied to substrates. This new analysis has been used to interpret literature data [15] on the density of cracks as a function of applied strain in brittle coatings applied to an aluminum substrate. We also describe some experiments on multiple cracking in relatively brittle poly(methyl methacrylate) coatings applied to ductile polycarbonate polymeric substrates. These experiments have been analyzed using the new fracture mechanics analysis of coating failure.

## MATERIALS AND METHODS

Experiments on failures of coatings were done using a model system of a poly(methyl methacrylate) (PMMA) coating applied to a General Electric Lexan<sup>®</sup> polycarbonate substrate. The PMMA coating was supplied by the DuPont company as a 40% by weight solution of a proprietary grade PMMA in acetone and toluene solvents. The viscosity average molecular weight of the PMMA was determined using a Canon-Fanske viscometer to be 75,000 g/mol. This molecular weight is about one order of magnitude less the the molecular weight of commercial PMMA such as Lucite<sup>®</sup> acrylic sheeting. The polycarbonate was purchased from Cadillac Plastics in the form of 3.175 mm (1/8 in) and 6.35 mm (1/4 in) thick sheets.

The PMMA coatings were applied to the polycarbonate sheets using a doctor blade (also know as film spreader or draw down bar). The PMMA coating was applied in multiple coats with each coat resulting in about 0.025 mm (1 mil) of additional coating thickness. The panels were dried in an oven at 60°C for about 20 minutes between coats. After the final coat, the panels were heat treated in an oven at 60°C to remove the solvents; air was circulated through the oven to aid in solvent removal. The heat treatment time required to remove all solvents was determined to be at least 7 days. Samples heat treated for less than 7 days gave irreproducible cracking results. Samples treated longer than 7 days gave large, clear cracks. All experiments reported in this paper are for panels heat-treated for at least 7 days.

Dog bone shaped specimens 115 mm (4.5 in) long that were 6.35 mm (1/4 in) wide in the narrow section were cut from the coated polycarbonate sheets. The dog bones were cut by first rough cutting on a band saw and then milling to final shape using a pin router and a dog bone shaped template. The router produced a high quality edge and did not induce any cracking in the PMMA coatings.

All experiments were done in tension on a 25 kN MTS System 810 servohydraulic testing frame. Applied strain was measured using an MTS extensometer. Stress-strain data was collected using an IBM PC and custom developed software that interfaced the IBM PC to an MTS 464 Digital Display Device. All experiments used a cross head rate of 0.05 mm/sec (0.118 in/min).

Tensile tests on uncoated polycarbonate and free PMMA film were done to determine those materials mechanical properties. The polycarbonate tests were done using dog bones that were cut by the same procedure used to cut coated polycarbonate sheets. Due to the brittle nature of thin PMMA films, it was not possible to prepare dog bone specimens and instead the tensile tests were

Table 1. Mechanical Properties of uncoated Lexan<sup>®</sup> polycarbonate and of free poly(methyl methacrylate) film. The measured properties were determined using a cross head speed of 0.05 mm/sec (0.118 in/min).

Property	Polycarbonate	Poly(methyl methacrylate)
Tensile Modulus (MPa)	2300	1700
Failure Elongation (%)	6 <sup>a</sup>	2.1 <sup>b</sup>
Poisson's Ratio	0.37 <sup>c</sup>	0.33 <sup>d</sup>

a. Elongation at initial load drop due to yielding

b. Elongation at complete fracture

c. General Electric product literature value - not measured

d. Assumed value - not measured

done using straight sided specimens. The free PMMA film was prepared by coating a thin sheet of Kapton<sup>®</sup> polyimide film. After coating, a straight sided specimen was cut out, and finally the free film was peeled off the Kapton<sup>®</sup> polyimide film. The poor adhesion between PMMA and Kapton<sup>®</sup> polyimide film made this procedure possible. The results of the tensile tests on polycarbonate and free PMMA film are given in Table 1.

The PMMA/polycarbonate coating cracking experiments were done using multiple tests on the same specimen. In each test, the specimen was loading to some prescribed strain, unloaded, and then the coating cracks were observed in a microscope. When the PMMA coating failed in large, clear cracks, those cracks could be observed by eye and were counted. The number of cracks in the gage length section of the dog bone specimen divided by the length of the gage length section gave the density of cracks at that strain. More details on the materials and methods can be found in ref. [22].

## ENERGY RELEASE RATE ANALYSIS

Consider the  $x$ - $z$  section of a coated substrate illustrated in Fig. 2. Layer 1 is the coating and it has modulus  $E_c$  and thickness  $t_1$ ; layers 2 and 3 are in the substrate and they each have modulus  $E_s$  and their thicknesses are  $t_2$  and  $t_3$ . The reason for splitting the substrate into two layers and where to make the split (*i.e.*, how to pick  $t_2$  and  $t_3$ ) will be described later. We will analyze for failure under axial loading. Before the cracks in Fig. 2 are formed and for a sample at the residual stress-free temperature,  $T_0$ , the stresses will be partitioned into each layer. By an equal strain assumption, the initial stresses will be:

$$\sigma_{x0}^{(1)} = \frac{E_c}{E_0} \sigma_0 \quad \text{and} \quad \sigma_{x0}^{(2)} = \sigma_{x0}^{(3)} = \frac{E_s}{E_0} \sigma_0 \quad (1)$$

where  $E_0$  is the modulus of the entire structure and  $\sigma_0$  is the applied axial stress.

Now change the temperature from  $T_0$  to  $T_s$  (where  $T_s$  is the specimen or test temperature) and form the two cracks at  $x = \pm a$  shown in Fig. 2. The stresses in each layer will change. In particular, there will be residual thermal stresses, transverse stresses, and shear stresses in each layer. We make one, and only one assumption about the form of the new stress state. We assume that the  $x$  axis tensile stresses in each layer depend only on the  $x$  coordinate and are independent of the  $z$  axis or thickness direction. By this assumption, the stresses in the three layers will change to:

## Multiple cracking in coatings

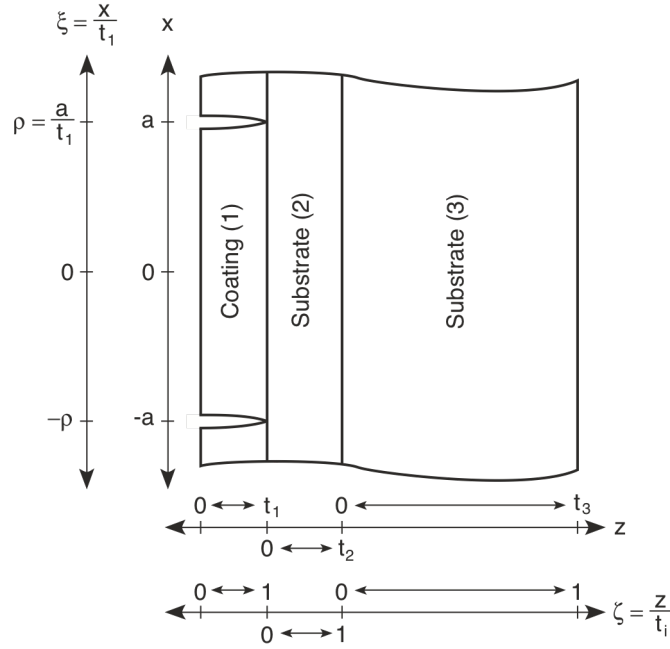


Fig. 2: The coordinate system between two cracks located at  $x = \pm a$  in the coating (layer 1). The substrate is divided into two layers - layers 2 and 3. The axial direction is the  $x$  axis and the thickness direction is the  $z$  axis. The  $\xi$  and  $\zeta$  directions are dimensionless directions located along the  $x$  and  $z$  axes, respectively.

$$\sigma_x^{(1)} = \sigma_{x0}^{(1)} - \psi_i(x) \quad (2)$$

where  $i = 1, 2$ , or  $3$ , and  $\psi_i(x)$  are three as yet undetermined functions of  $x$ . By using equilibrium equations, requiring the free edge stresses to be zero, requiring the transverse and shear stresses to be continuous across layer boundaries, and requiring force balance, it is possible to reduce the stresses in all layers to a form that is dependent on only one undetermined function of  $x$ :

$$\sigma_x^{(1)} = \sigma_{x0}^{(1)} - \psi f_i'' \quad (3)$$

$$\sigma_{xz}^{(1)} = \psi' f_i' \lambda_i \quad (4)$$

$$\sigma_z^{(1)} = -\psi'' f_i \lambda_i^2 \quad (5)$$

where  $\psi = \psi_1(\xi)$ ,  $\xi$  is the dimensionless coordinate  $\xi = x/t_1$ ,  $\lambda_i = t_i/t_1$ , and the three functions,  $f_i$ , are functions of the dimensionless coordinate  $\zeta = z/t_i$ :

$$f_1 = \frac{1}{2} \zeta^2 \quad (6)$$

$$f_2 = \frac{1}{2\lambda_2^2} + \frac{\zeta}{\lambda_2} - \frac{(1+R)}{2\lambda_2} \zeta^2 \quad (7)$$

$$f_3 = \frac{R}{2\lambda_3} (\zeta - 1)^2 \quad (8)$$

In these equations,  $z$  in layer  $i$  goes from 0 to  $t_i$  and therefore  $\zeta$  goes from 0 to 1, and the term  $R$  is

$$R = \frac{1 + \lambda_2}{\lambda_2 + \lambda_3} \quad (9)$$

The derivation of Eqs. (3) - (8) is a straightforward extension of the derivations given in Refs. [18], [20], and [21]; the reader is referred to those papers for details. Finally, the reason for splitting the substrate layer into two layers is that with only one layer we could not have derived a stress state that meets the assumption in eq. (2) while simultaneously meeting all the boundary and stress continuity conditions. In other words, the extra layer was required to provide an extra degree of freedom.

As can be verified by substitution, the stress state in Eqs. (3) - (5) satisfies equilibrium, traction boundary conditions, and interface stress continuity, and is therefore an admissible stress state. By the principal of minimum complementary energy, the function,  $\psi$ , which produces the minimum value for the complementary energy will give the best approximation to the coated substrate stress state. The function  $\psi$  is found by plugging the admissible stress state into the complementary energy function and finding the minimum by using the calculus of variations. For thermoelastic analyses, a variational solution based on the principal of minimum complementary energy is found by minimizing the function  $\Gamma$  given by:

$$\Gamma = \frac{1}{2} \int_V \boldsymbol{\sigma} \cdot \mathbf{K} \boldsymbol{\sigma} dV + \int_V \boldsymbol{\sigma} \cdot \boldsymbol{\alpha} T dV + \int_{S_1} \boldsymbol{\sigma} \cdot \hat{\mathbf{u}} dS \quad (10)$$

where  $\boldsymbol{\sigma}$  is the stress tensor,  $\mathbf{K}$  is the compliance tensor,  $\boldsymbol{\alpha}$  is the thermal expansion coefficient tensor,  $T$  is  $T_s - T_0$ ,  $V$  is the volume of the sample, and  $S_1$  is that part of the sample subjected to fixed displacement of  $\hat{\mathbf{u}}$  [23]. In this problem  $S_1$  is null.

We evaluate  $\Gamma$  for the region between two coating cracks; *i.e.* for the region  $-\rho < \xi < \rho$  and  $0 < \zeta < 1$  within each layer. The plane stress solution will be obtained by using the  $\mathbf{K}$  and  $\boldsymbol{\alpha}$  tensors (in contracted form):

$$\mathbf{K} = \begin{pmatrix} \frac{1}{E_i} & -\frac{\nu_i}{E_i} & 0 \\ -\frac{\nu_i}{E_i} & \frac{1}{E_i} & 0 \\ 0 & 0 & \frac{1}{G_i} \end{pmatrix} \quad \text{and} \quad \begin{pmatrix} \alpha_i \\ \alpha_i \\ 0 \end{pmatrix} \quad (11)$$

where  $E_i$ ,  $G_i$ ,  $\nu_i$ , and  $\alpha_i$  are the tensile modulus, shear modulus, Poisson's ratio, and thermal expansion coefficient, respectively, for layer  $i$ . We will discuss only the plane-stress solution as the plane-strain solution may be obtained from the plane-stress solution by substituting reduced mechanical properties:

$$E_{ir} = \frac{E_i}{1 - \nu_i^2}, \quad \nu_{ir} = \frac{\nu_i}{1 - \nu_i}, \quad G_{ir} = \frac{E_{ir}}{2(1 + \nu_{ir})}, \quad \text{and} \quad \alpha_{ir} = (1 + \nu_i)\alpha_i \quad (12)$$

Substituting in the stresses in Eqs. (3)-(5) and evaluating the  $\zeta$  integrals using the procedures described in Refs. [18-21] results in:

$$\Gamma = \Gamma_0 + t_1^2 \int_{-\rho}^{\rho} [C_1 \psi^2 + C_2 \psi \psi'' + C_3 \psi''^2 + C_4 \psi'^2 + C_5 \psi'' + C_6 \psi] d\xi \quad (13)$$

where

$$\Gamma_0 = \sum_{i=1}^3 t_1^2 \lambda^i \int_{-\rho}^{\rho} \left( \frac{\sigma_{x0}^{(i)2}}{2E_i} + \alpha_i \sigma_{x0}^{(i)} T \right) d\xi \quad (14)$$

$$C_1 = \frac{1}{2} \left[ \frac{1}{E_c} + \frac{1}{E_s} \left( \frac{(1+R)^2}{\lambda_2} + \frac{R^2}{\lambda^2} \right) \right] \quad (15)$$

$$C_2 = \frac{1}{6} \left[ -\frac{\nu_c}{E_c} + \frac{\nu_s}{E_s} \left( (1+R)(3 + \lambda_2(2-R)) - \lambda_3 R^2 \right) \right] \quad (16)$$

$$C_3 = \frac{1}{120} \left[ \frac{3}{E_c} + \frac{1}{E_s} \left( \lambda_2^3(8 - 9R + 3R^2) + \lambda_2^2(20 - 10R) + 15\lambda_2 + 3R^2\lambda_3^3 \right) \right] \quad (17)$$

$$C_4 = \frac{1}{6} \left[ \frac{1}{G_c} + \frac{1}{G_s} \left( \lambda_2(R^2 - R + 1) + \lambda_3 R^2 \right) \right] \quad (18)$$

$$C_6 = -(\alpha_c - \alpha_s)T = -\Delta\alpha T \quad (19)$$

and  $C_5$  is not needed because from the boundary condition of zero shear stresses on the crack surfaces

$$\int_{-\rho}^{\rho} \psi'' d\xi = 0 \quad (20)$$

The result in eq. (13) is identical to the analogous result in ref. [18] (*cf.* eq. (14) in ref. [18]) except that the constants  $C_1$  to  $C_6$  are different. The solution to the calculus of variation problem that yields  $\psi$  can therefore be quoted directly from ref. [18]; the function  $\psi$  that minimizes the complementary energy is

$$\psi = \left( \sigma_{x0}^{(1)} + \frac{C_6}{2C_3} \right) \phi - \frac{C_6}{2C_3} \quad (21)$$

where  $\phi$  is function that depends on the sign of  $4q/p^2 - 1$  where  $p = (C_2 - C_4)/C_3$  and  $q = (C_1/C_3)$ . When  $4q/p^2$  is greater than 1:

$$\begin{aligned} \phi = & \frac{2(\beta \sinh \alpha \rho \cos \beta \rho + \alpha \cosh \alpha \rho \sin \beta \rho)}{\beta \sinh 2\alpha \rho + \alpha \sin 2\beta \rho} \cosh \alpha \xi \cos \beta \xi \\ & + \frac{2(\beta \cosh \alpha \rho \sin \beta \rho + \alpha \sinh \alpha \rho \cos \beta \rho)}{\beta \sinh 2\alpha \rho + \alpha \sin 2\beta \rho} \sinh \alpha \xi \sin \beta \xi \end{aligned} \quad (22)$$

where

$$\alpha = \frac{1}{2} \sqrt{2\sqrt{q} - p} \quad \beta = \frac{1}{2} \sqrt{2\sqrt{q} + p} \quad (23)$$

When  $4q/p^2$  is less than 1 (and  $p < 0$  and  $q > 0$  as they always are):

$$\begin{aligned} \phi = & \frac{\beta \cosh \alpha \xi}{\sinh \alpha \rho (\beta \coth \alpha \rho - \alpha \coth \beta \rho)} \\ & + \frac{\alpha \cosh \beta \xi}{\sinh \beta \rho (\alpha \coth \beta \rho - \beta \coth \alpha \rho)} \end{aligned} \quad (24)$$

where

$$\alpha = \sqrt{-\frac{p}{2} + \sqrt{\frac{p^2}{4} - q}} \quad \beta = \sqrt{-\frac{p}{2} - \sqrt{\frac{p^2}{4} - q}} \quad (25)$$

One feature of the coatings analysis that differs from the composite analysis in ref. [18] is that we must choose where to divide the substrate layer into two separate layers. The best method is to use the principal of minimum complementary energy and select the division line at the location that minimizes the complementary energy. The procedure is to minimize  $\Gamma$  with respect to the choice of  $\lambda_2$  (which determines  $\lambda_3$ ) where the  $\psi$  function that minimizes  $\Gamma$  for any particular value of  $\lambda_2$  is always given by eq. (21). Unlike the minimization to find  $\psi$ , the minimization to find  $\lambda_2$  can not be done analytically. Instead, we resorted to numerical procedures. The numerical results can be summarized as follows: as long as the coating thickness is not large (*i.e.*, its thickness is much less than the substrate thickness), the value of  $\lambda_2$  that minimizes the complementary energy is close to 1. In other words, the thickness of layer 2 should be set equal to the thickness of the coating or layer 1. Layer 2 can be said to be a stress concentration layer that includes most of the disturbances to the stresses in the substrate that result from cracks in the coating. The minimum complementary energy is produced when the range of stress disturbance is the same size as the crack. When the thickness of layer 2 is equal to the thickness of the coating:

$$\lambda_1 = \lambda_2 = 1, \quad \lambda_3 = \lambda \quad \text{and} \quad R = \frac{2}{1 + \lambda} \quad (26)$$

and the expressions for  $C_1$  to  $C_4$  in Eqs. (15) to (18) can be simplified.

Before embarking of the multiple cracking fracture analysis, we include three more useful results from ref. [18]. Consider the sample in Fig. 3A which has  $N$  crack intervals characterized by crack spacings  $\rho_1, \rho_2, \dots, \rho_N$ . The sample compliance is (*cf.* eq. (38) in ref. [18])

$$C = C_0 + \frac{E_c^2}{E_0^2} \frac{2C_1 t_1 L}{B^2 W} \frac{\sum_{i=1}^N \chi(\rho_i)}{\sum_{i=1}^N \rho_i} \quad (27)$$

where  $B = t_1 + t_2 + t_3$  is the total thickness,  $W$  is the sample width,  $L$  is the sample length and  $C_0 = L/(BE_0W)$  is the compliance of the uncracked sample. The new function  $\chi(\rho)$  depends on the sign of  $4q/p^2 - 1$ . When  $4q/p^2$  is greater than 1:

$$\chi(\rho) = 2\alpha\beta (\alpha^2 + \beta^2) \frac{\cosh 2\alpha\rho - \cos 2\beta\rho}{\beta \cosh 2\alpha\rho + \alpha \sin 2\beta\rho} \quad (28)$$

When  $4q/p^2$  is less than 1:

$$\chi(\rho) = \alpha\beta (\beta^2 - \alpha^2) \frac{\tanh \beta\rho \tanh \alpha\rho}{\beta \tanh \beta\rho - \alpha \tanh \alpha\rho} \quad (29)$$

The total strain energy in the  $N$  crack intervals is (*cf.* eq. (43) in ref. [18])

$$U = \left( \frac{\sigma_0^2}{2E_0} + \frac{t_1 C_6^2}{4C_1 B} \right) BWL + (C - C_0) \frac{E_0^2}{E_c^2} \frac{B^2 W^2}{2} \left( \frac{E_c^2}{E_0^2} \sigma_0^2 - \frac{C_6^2}{4C_1^2} \right) \quad (30)$$

Note that there are no coupling terms in the strain energy involving both the applied stresses and the residual thermal stresses. The coupling terms were not omitted; for this specific stress state the

### Multiple cracking in coatings

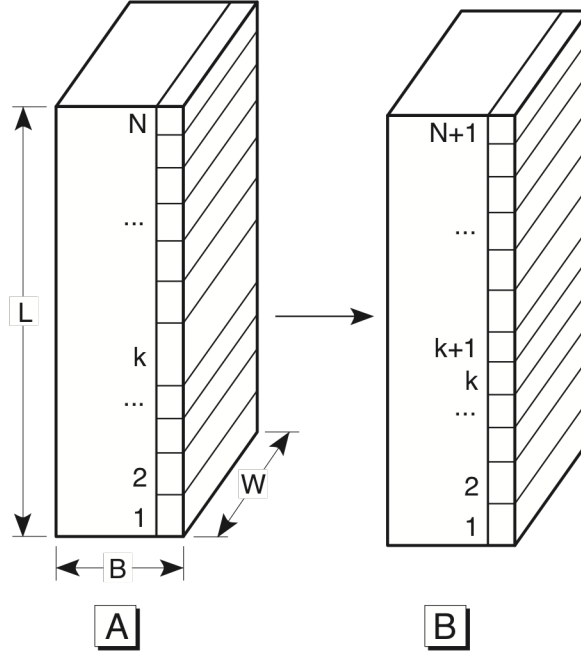


Fig. 3: Sample A has  $N$  cracks with crack spacings  $\rho_1, \rho_2, \dots, \rho_N$ . Sample B has a new crack located in the  $k^{\text{th}}$  crack interval of sample A. Sample length ( $L$ ), thickness ( $B$ ), and width ( $W$ ) are shown on sample A.

coupling terms cancel to zero. Finally, the longitudinal thermal expansion coefficient of the cracked sample is

$$\alpha_L = \alpha_L^0 - \frac{C - C_0}{C_0} \frac{\Delta\alpha}{2C_1 E_c} \quad (31)$$

where  $\alpha_L^0$  is the thermal expansion coefficient of the uncracked sample.

By the energy approach to multiple cracking in coatings, we assume that the next coating crack will form when the energy released on forming that crack reaches the fracture toughness of the coating. Consider the formation of a crack in the  $k^{\text{th}}$  crack interval as shown in Fig. 3B. The energy release rate on forming this crack can be found by differentiating eq. (30) with respect to total coating crack area,  $A$ , at constant displacement [18]:

$$G = - \left. \frac{dU}{dA} \right|_{\text{const } u} = \frac{E_0^2 B^2 W^2}{E_c^2} \frac{1}{2} \left( \frac{E_c}{E_0} \sigma_0 + \frac{C_6}{2C_1} \right)^2 \frac{dC}{dA} \quad (32)$$

In deriving eq. (32) we needed to evaluate  $d\sigma_0/dA|_{\text{const } u}$ . Using the relation for sample compliance times load of

$$CP = u(P) - \underline{u}(0) = u(P) - \alpha_L LT \quad (33)$$

where  $u(P)$  is sample displacement under load  $P$ , and differentiating results in

$$\left. \frac{d\sigma_0}{dA} \right|_{\text{const } u} = \left( -\frac{\sigma_0}{C} + \frac{E_0}{E_c} \frac{\Delta\alpha T}{2C_1 C} \right) \frac{dC}{dA} \quad (34)$$

Equation (34) corrects an error in ref. [18] (see eq. (44) in ref. [18]) and accounts for the difference between eq. (32) and the corresponding equation in ref. [18].

Evaluating  $dC/dA$  by differentiating eq. (27) results in the final energy release rate expression:

$$G = \left( \frac{E_c}{E_0} \sigma_0 + \frac{C_6}{2C_1} \right)^2 C_3 t_1 Y(D) \quad (35)$$

where  $Y(D)$  is a calibration function that depends on the crack density,  $D = N/L$ , or more formally on the complete distribution of crack spacings:

$$Y(D) = LW \frac{d}{dA} \frac{\sum_{i=1}^N \chi(\rho_i)}{\sum_{i=1}^N \rho_i} = 2 \frac{d}{dD} (D \langle \chi(\rho) \rangle) \quad (36)$$

where  $\langle \chi(\rho) \rangle$  is the average value of  $\chi(\rho)$  over the  $N$  crack spacings.

To use eq. (35), we must evaluate  $Y(D)$ . For the fracture process illustrated in Fig. 3 where a new crack forms in the center of the  $k^{\text{th}}$  interval, we can evaluate  $Y(D)$  using a discrete differentiation. Before the crack forms  $\langle \chi(\rho) \rangle = (1/N) \sum_{i=1}^N \chi(\rho_i)$  and  $D = N/L$ . After the crack forms in  $\langle \chi(\rho) \rangle = (1/(N+1)) (\sum_{i=1}^N \chi(\rho_i) - \chi(\rho_k) + 2\chi(\rho_k/2))$  and  $D = (N+1)/L$ . The calibration function is then:

$$Y(D) = 2 \frac{\Delta(D \langle \chi(\rho) \rangle)}{\Delta D} = 2(2\chi(\rho_k/2) - \chi(\rho_k)) \quad (37)$$

During a typical experiment we will not know the location of the next crack. Because multiple cracking tends to form itself into regular arrays, however, we assume that the next crack will form in a crack interval whose spacing is close to the average spacing. In other words when the crack density is  $D$ , the next crack will form in a crack interval whose spacing is  $\rho = 1/(2t_1 D)$  and the calibration function is given by

$$Y(D) = 2(2\chi(\rho/2) - \chi(\rho)) = 2 \left[ 2\chi \left( \frac{1}{4t_1 D} \right) - \chi \left( \frac{1}{2t_1 D} \right) \right] \quad (38)$$

Finally, we consider the formation of the first crack. The energy release rate for the first crack is

$$G = \left( \frac{E_c}{E_0} + \frac{C_6}{2C_1} \right)^2 C_3 t_1 \lim_{D \rightarrow 0} Y(D) \quad (39)$$

For the two solutions described above, when  $4q/p^2$  is less than 1:

$$\lim_{D \rightarrow 0} Y(D) = 4\alpha \sqrt{\frac{C_1}{C_3}} \quad (40)$$

and when  $4q/p^2$  is less than 1:

$$\lim_{D \rightarrow 0} Y(D) = 2(\alpha + \beta) \sqrt{\frac{C_1}{C_3}} \quad (41)$$

## RESULTS AND DISCUSSION

Eqs. (39) and (35) are aimed at predicting the formation and multiplication of cracks in coatings. Given a coating with a particular fracture toughness,  $G_c$ , we can solve eq. (39) for applied stress. The calculated applied stress should be the stress required to cause the first crack in the coating. As the stress is increased above this threshold stress, the density of coating cracks should increase. For a given coating toughness and crack density, we can solve eq. (35) for applied stress and predict the stress required to produce that given crack density. In this section we compare the theoretical predictions to experimental results.

### *Cracking of Brittle Coatings used for Stress Analysis*

One historic use of brittle coatings has been for stress analysis of structures. The traditional interpretation of brittle coating results is that when the coating cracks, the strain in the structure at that location is equal to the critical strain to failure of the coating material. Unfortunately, as stated in the introduction, strength theories of coating failures do not work and there is no such thing as a critical strain to failure. The failure of strength based theories can be demonstrated by measuring the critical strain to cracking as a function of coating thickness. The strain to failure is not a material constant but depends on the coating thickness with thicker coatings cracking at lower strains [15]. For this reason, brittle coating stress analysis results must always be interpreted using calibration substrates loaded to known strains to which the same coating has been applied with the same thickness and under the same conditions.

A common experiment for calibrating brittle coatings is to apply the coating to a metal substrate and bend the sample as a cantilever beam. Under these conditions, brittle coatings typically give multiple transverse cracks similar to those illustrated in Fig. 1. By recording the location of the cracks and applying simple linear beam theory, it is possible to measure the strain to initial failure and the density of cracks as a function of applied strain. These type of experiments were used by Durelli *et. al.* [15] to measure the crack density as a function of applied strain in Stresscoat No. 1206 brittle coating applied to an aluminum substrate. The substrate thickness was 6.35 mm (1/4 in) thick and the coating thickness was varied from 0.091 mm (3.6 mils) to 0.295 mm (11.6 mils) [15]. We attempted to fit these experimental results to the energy release rate analysis in the previous section. One problem is that the experiments were done in bending and our analysis is for tensile loading. We note, however, that most of the energy released in our analysis is released from the coating and from the stress concentration layer. Because these two layers are thin layers located near the outer edge of the cantilever beam, they will be under a state of relatively uniform axial strain. Faced with a lack of alternative literature data, we assumed that the tensile stress analysis can be used to interpret data obtained during bend tests. Some possible consequences of this assumption will be discussed later.

We attempted to fit the Durelli *et. al.* [15] crack density data for the thinnest ( $t_1 = 0.091$  mm (3.5 mils)) and for the thickest ( $t_1 = 0.295$  mm (11.6 mils)) coatings. We selected a value for the coating toughness and then using eq. (35) with  $Y(D)$  given by eq. (38) solved for the strain required to produce a given crack density. Inverting this solution gave the crack density as a function of applied strain. The value of the coating toughness was then varied until we simultaneously obtained the best fit to the data for both coating thicknesses. Figure 4 shows the fit obtained using a coating toughness of 160 MJ/m<sup>2</sup>. The material properties used to generate this fit were supplied in ref. [15] ( $E_c = 2140$  MPa,  $\nu_c = 0.42$ ,  $E_s = 72000$  MPa,  $\nu_s = 0.31$ ,  $t_s = 6.35$  mm

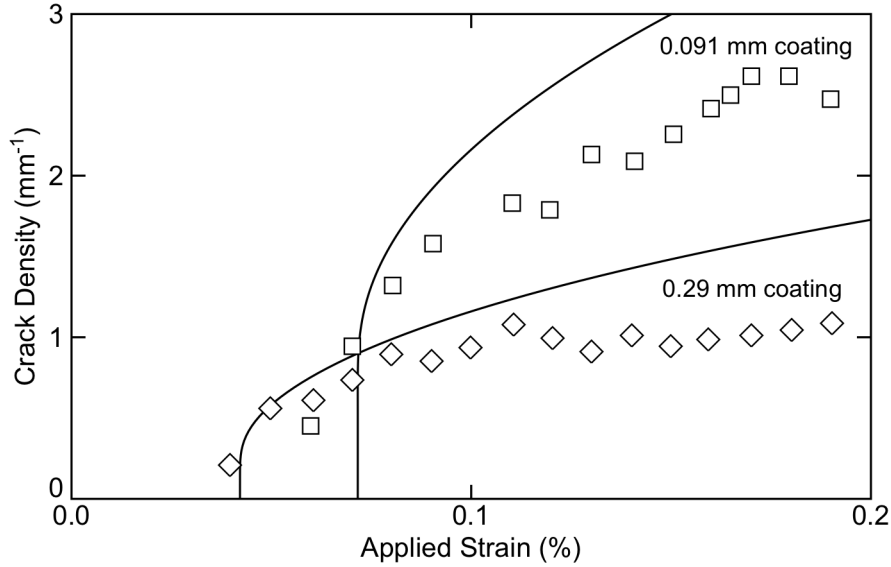


Fig. 4: The crack density as a function of applied load for Stresscoat No. 1206 brittle stress analysis coating as a function of applied strain. The experimental data points are for samples with coatings of thicknesses 0.091 mm (3.6 mils) and 0.295 mm (11.6 mils). The smooth lines are predictions using eq. (35) and a critical energy release rate of  $160 \text{ mJ/m}^2$ .

(1/4 in)); due to lack of information, the residual thermal stresses were assumed to be negligible and  $T$  was set to zero.

We claim that the fits in Fig. 4 are good. The key features of the experimental results are:

1. The thick coating cracks at a lower strain than the thin coating.
2. After initial cracking the thin coating multiply cracks to a higher crack density than the thick coating.
3. Both the thick coating and the thin coating show a rapid increase in number of cracks immediately after the first crack forms. After the first few cracks, the rate of crack multiplication decreases.

The theoretical fits reproduce all these features. Thus, with knowledge of the coating toughness, eq. (35) can be used to predict all trends in coating cracking as a function of the coating thickness. In other words, unlike the critical strain to failure, the coating fracture toughness is a useful material property. On close inspection, the experimental results fall below the theoretical predictions at high applied strain. Two possible explanations for the discrepancies are:

1. The analysis was for tensile loading and the experiments were done in bending. The differences in loading conditions cast doubt on the meaning of the substrate thickness. If we treat the substrate thickness as an adjustable parameter, we can fit the data at high strains without affecting the fit at low strains simply by assuming a thicker substrate. In other words, a coating on a substrate loaded in bending acts as if it is a coating on a thicker substrate that is loaded in tension.
2. At high strains other failure modes, such as delamination of the coating from the substrate or yielding of the aluminum substrate, may be occurring. If the coating

## Multiple cracking in coatings

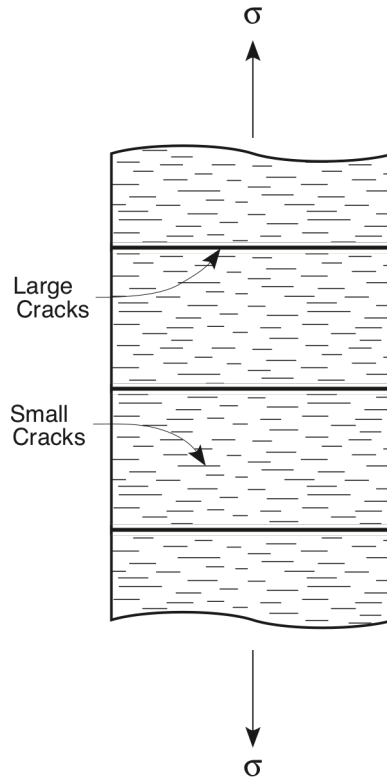


Fig. 5: Cracking pattern in most poly(methyl methacrylate) coatings on a polycarbonate substrate. The coating fails in large clear cracks and there are typically small microcracks located between the large cracks.

delaminates before complete multiple cracking, for example, then the final extent of multiple cracking will be less than if the coating never delaminates.

### *Acrylic Coating on Polycarbonate*

Polycarbonate sheets coated with PMMA as described in the Materials and Methods section were loaded in tension and the cracking of the PMMA coating was observed. Adequately heat-treated samples showed large, clear cracks running across the sample width as illustrated in Fig. 1. Most of the samples showed an additional type of cracking in the form of microcracks located between the large cracks. A typical pattern of coating failure is illustrated in Fig. 5. The large cracks were visible by eye while the microcracks were only visible under a microscope. These microcracks were not observed in brittle stress analysis coatings [15] and are not currently accounted for in the energy release rate analysis.

Our first analysis of PMMA coating cracking was to consider only the formation of the first large crack. We measured the strain to cause the first clear crack as a function of the PMMA coating thickness. The experimental results along with a fit using eq. (39) are plotted in Fig. 6. The theoretical line was a best fit obtained using a coating toughness of  $G_c = 420 \text{ J/m}^2$ . The mechanical properties of the coating and substrate are listed in Table I. All these experiments were done using 3.175 mm (1/8 in) thick substrates. Finally, by coating PMMA onto a thin polycarbonate sheet under the same conditions used to coat the thick polycarbonate sheets, and observing the resulting

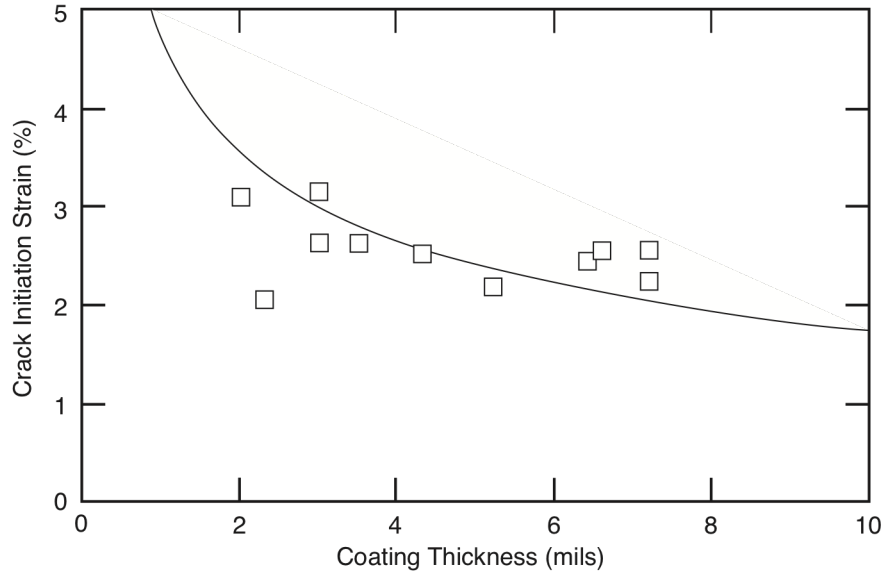


Fig. 6: The strain required to form the first large clear crack in a poly(methyl methacrylate) coating on a polycarbonate substrate as a function of the thickness of the coating. The symbols are experimental results and the smooth line is the prediction using eq. (39) and a critical energy release rate of  $420 \text{ J/m}^2$ .

curvature, we determined that the level of residual stresses in the coating was negligible compared to the applied stress. To account for negligible residual stresses,  $T$  was set to 0.

There is significant scatter in the strain to first crack data, but with the exception of one point (lower left most point) the data is reasonable well predicted by eq. (39). The general trend is that the thicker coatings crack at a slightly lower strain. Note that no sample fails at a strain that is as low as the strain to failure of the free film which was 2.1%. More significant than the quality of fit is the absolute value of the coating toughness of  $420 \text{ J/m}^2$ . General grade poly(methyl methacrylate) toughness has been reported to be  $220$  to  $510 \text{ J/m}^2$  [24] and  $500 \text{ J/m}^2$  [25]. The value from coating cracking experiments of  $420 \text{ J/m}^2$  is in line with expectations for PMMA.

Interpretation of the density of cracks as a function of strain for polycarbonate/PMMA samples was complicated by the presence of the microcracks. Because it would be very difficult to determine a crack density that included the microcracks, we choose to ignore the microcracks and determine the crack density based solely on the number of large cracks. Typical results are shown in Fig. 7 for a sample with a PMMA coating thickness of  $0.089 \text{ mm}$  (3.5 mils). Figure 7 gives experimental data and the predicted crack density for a coating whose toughness in  $400 \text{ J/m}^2$ . The coating toughness of  $400 \text{ J/m}^2$  accurately predicts the onset of cracking but dramatically over estimates the extent of cracking at high applied strains. We speculate that the microcracks interfere with the full development of multiple cracking.

For unexplained reasons, one sample showed large cracks and no microcracks. Figure 8 shows the experimental data for this sample and the predicted crack density for a coating whose toughness is  $500 \text{ J/m}^2$ . The thickness of the PMMA coating on this sample was  $0.076 \text{ mm}$  (3.0 mils). The observation that this sample is well predicted by theory adds weight to our speculation that the problem with the other experiments (e.g. Fig. 7) is related to the presence of microcracking. The quality of the fit to the experimental data points further supports the applicability of eq. (35).

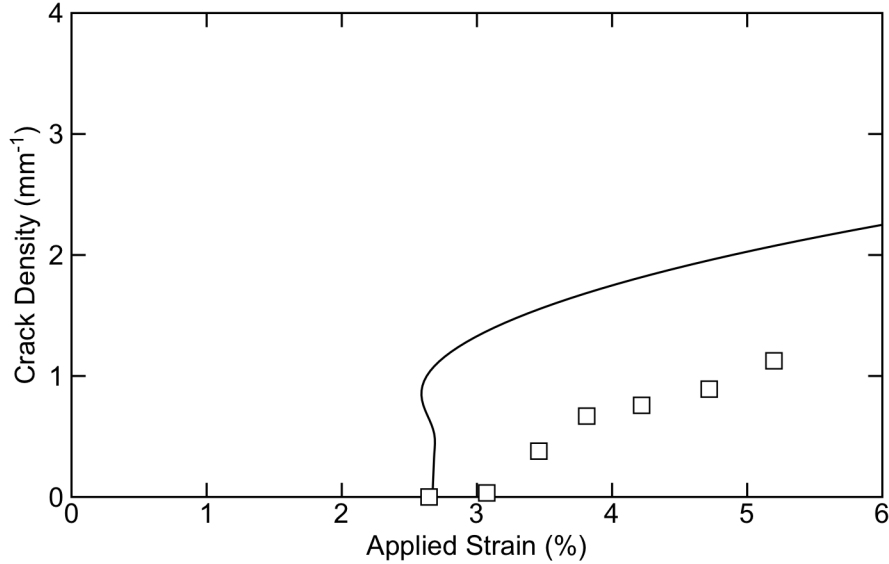


Fig. 7: The crack density as a function of applied load for a poly(methyl methacrylate) coating on a polycarbonate substrate as a function of applied strain. The experimental data points are for a sample with a coating thickness of 0.089 mm (3.5 mils) on a 3.175 mm (1/8 in) substrate. The smooth line is a prediction using eq. (35) and a critical energy release rate of 400 J/m<sup>2</sup>.

Although the theory can only fit PMMA coating cracking data when the coating happens to fail with only large cracks, we note that even the samples that do fail with microcracks show all the key features predicted by eq. (32). In other words, all experimental results show a rapid increase in crack density immediately after formation of the first crack followed by a leveling off at higher applied strains.

## CONCLUSIONS

A new stress analysis of cracked coatings based on variational mechanics has been developed. The new analysis was used to derive the energy released due to the formation of a new crack in a coating. If we assume an energy based failure model, the new analysis can be used to predict multiple cracking failures of brittle coatings applied to substrates. The key predictions are that soon after the initiation of the first coating crack, the crack density will rapidly increase and that at higher strains the crack density will increase at a slower rate. Another prediction is that thicker coatings will crack before thin coatings but that the thin coatings will eventually develop a higher density of cracks.

All predictions of the new theory are in line with experimental data of cracking of coatings. When theory is compared to actual experiments, the agreement is good. Despite good agreement, we sometimes observed deviations between experiment and theory. These deviations, however, can be explained either by test conditions or by sample failure mechanism. The discrepancy between the theory and the crack density in brittle coatings was probably due to the experiments being done in bending while the theory was derived for tensile loading. The failure of the theory to fit data for some PMMA/polycarbonate samples could be attributed to the presence of small

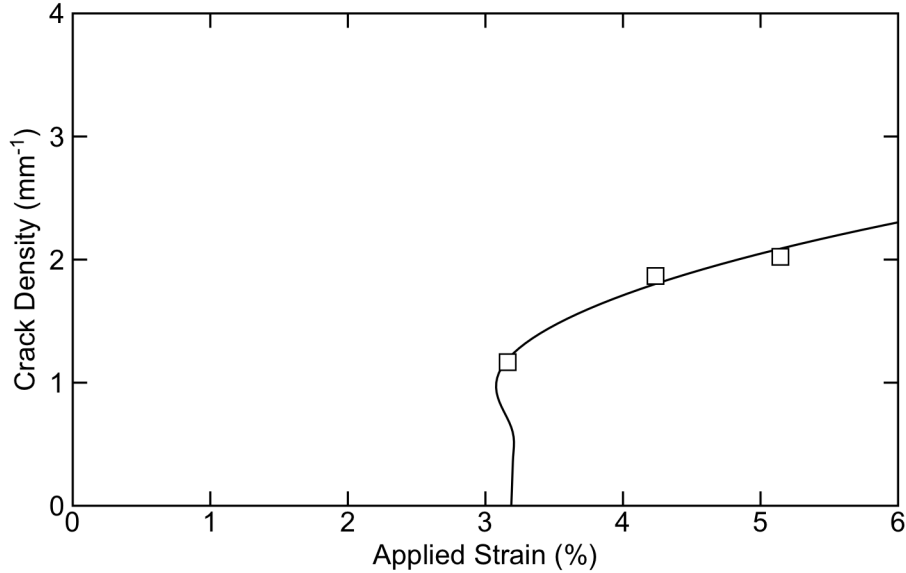


Fig. 8: The crack density as a function of applied load for a poly(methyl methacrylate) coating on a polycarbonate substrate as a function of applied strain. The experimental data points are for a sample with a coating thickness of 0.076 mm (3.0 mils) on a 3.175 mm (1/8 in) substrat. The smooth line is a prediction using eq. (35) and a critical energy release rate of 500 J/m<sup>2</sup>.

microcracks between the large clear cracks. When the small microcracks were absent, the agreement with theory was good.

We can suggest some possible uses for this new analysis of cracking in coatings. First, experiments similar to those described in this paper in conjunction with analysis using eq. (35) or (39) can be used to measure the *in situ* fracture toughness of coatings. Because the *in situ* coating fracture toughness is independent of non-material parameters (e.g. coating thickness) it is fundamental material property characterizing the toughness of a coating. An alternative measure of coating toughness is to undertake standard fracture mechanics characterization of the coating as a free film. Standard fracture mechanics procedures, however, may require relatively thick samples [26] for valid test results. The coating may not be obtainable in thick form or may not be obtainable in a thick form whose morphology is similar to the coating as applied in thin layers to a substrate. Even if thick coatings can be obtained, we suggest that the *in situ* coating toughness measured using the procedures in this paper will be more likely to correlate with coating performance than will fracture toughness measurements on the coating as a free film. When measuring the *in situ* coating toughness, interactions with the substrate are automatically taken into account.

Another use of the fracture theory is to predict changes in coating performance due to changes in external variables. In principle, the energy release rate includes the effect of coating thickness, substrate thickness, coating properties, substrate properties, and residual stresses. The experimental results in this paper show that it correctly predicts the effect of substrate thickness. Although not backed by experimental results, we expect will also predict the the effects of the other variables. Perhaps most important is the effect of residual stresses. Experiments on coatings as free films will never yield information on the performance in the presence of residual stresses. In contrast, fracture experiments on coatings applied to substrates in such a manner that those coatings are placed under residual stress can yield information on the effect of residual stresses.

Eqs. (35) and (39) include a residual stress term and therefore provide an energy release rate analysis of failure in the presence of residual stresses.

*Acknowledgement*—This work was supported in part by a contract from the Marshall R&D Laboratory, Automotive Products Department, E. I. duPont deNemours & Company monitored by Paul J. McGonigal.

## REFERENCES

1. R. O. Carhart, D. A. Davis, and R. Giuffria, *SPE Journal*, April, 440 (1962).
2. P. So and L. J. Broutman, *Polym. Eng. & Sci.*, **22**, 888 (1982).
3. L. Rolland and L. J. Broutman, *Polym. Eng. & Sci.*, **25**, 207 (1985).
4. H. T. Hahn and S. W. Tsai, *J. Comp. Mat.*, **8**, 288 (1974).
5. K. W. Garrett and J. E. Bailey, *J. Mat. Sci.*, **12**, 157 (1977).
6. K. W. Garrett and J. E. Bailey, *J. Mat. Sci.*, **12**, 2189 (1977).
7. A. L. Highsmith and K. L. Reifsnider, *ASTM STP 775*, 103 (1982).
8. A. K. Parvizi, K. W. Garrett, and J. E. Bailey, *J. Mat. Sci.*, **13**, 195 (1978).
9. A. Parvizi and J. E. Bailey, *J. Mat. Sci.*, **13**, 2131 (1978).
10. M. G. Bader, J. E. Bailey, P. T. Curtis, and A. Parvizi, *Proc. 3<sup>rd</sup> Int'l Conf. on Mech. Behavior of Materials*, **3**, 227 (1979).
11. J. E. Bailey, P. T. Curtis and A. Parvizi, *Proc. Roy. Soc. London*, **A366**, 599 (1979).
12. P. W. Manders, T. W. Chou, F. R. Jones, and J. W. Rock, *J. Mat. Sci.*, **18**, 2876 (1983).
13. H. Fukunaga, T. W. Chou, P. W. M. Peters, and K. Schulte, *J. Comp. Mat.*, **18**, 339 (1984).
14. D. L. Flagg and M. H. Kural, *J. Comp. Mat.*, **16**, 103 (1982).
15. A. J. Durelli, E. A. Phillips, and C. H. Tsao, *Analysis of Stress and Strain*, chapter 16 (McGraw-Hill, New York, 1958).
16. D. L. Flagg, *J. Comp. Mat.*, **19**, 29 (1985).
17. Y. M. Han, H. T. Hahn, and R. B. Croman, *Proc. of the Amer. Soc. Composites, Second Technical Conf.*, Newark, DE (September 23-25, 1987).
18. J. A. Nairn, *J. Comp. Mat.*, **23**, 1106 (1989).
19. J. A. Nairn, *Proc. of the Amer. Soc. Composites, Third Technical Conf.*, Seattle, WA (September 25-29, 1988).
20. Z. Hashin, *Mechanics of Materials*, **4**, 121 (1985).
21. Z. Hashin, *Eng. Fract. Mech.*, **25**, 771 (1986).
22. S. R. Kim, *Fracture Mechanics Approach to Multiple Cracking in Paint Films*, M.S. Thesis, University of Utah, August, 1989.
23. D. E. Carlson, in *Mechanics of Solids: Volume II*, C. Truesdell, ed., p. 325 (Springer-Verlag, Berlin, 1984).
24. J. G. Williams, *Fracture Mechanics of Polymers*, (John Wiley & Sons, New York, 1984).
25. J. P. Berry, *J. Polym. Sci.*, **50**, 107 (1961).
26. ASTM E399 (1983)

(Received 4 January 1990)